Experimental Evidence of Kinetic Effects in Indirect-Drive Inertial Confinement Fusion Hohlraums

L. Q. Shan,[1] H. B. Cai,[2,3,4,*] W. S. Zhang,[5] Q. Tang,[1] F. Zhang,[1] Z. F. Song,[1] B. Bi,[1] F. J. Ge,[2] J. B. Chen,[1] D. X. Liu,[1] W. W. Wang,[1] Z. H. Yang,[1] W. Qi,[1] C. Tian,[1] Z. Q. Yuan,[1] B. Zhang,[1] L. Yang,[1] J. L. Jiao,[1] B. Cui,[1] W. M. Zhou,[1,4] L. F. Cao,[1] C. T. Zhou,[2] Y. Q. Gu,[1,4,†] B. H. Zhang,[1] S. P. Zhu,[2,1,5] and X. T. He[2,3,4]

[1]*Science and Technology on Plasma Physics Laboratory, Research Center of Laser Fusion, CAEP, Mianyang 621900, China*

[2]*Institute of Applied Physics and Computational Mathematics, Beijing 100094, China*

[3]*HEDPS, Center for Applied Physics and Technology, Peking University, Beijing 100871, China*

[4]*IFSA Collaborative Innovation Center, Shanghai Jiao Tong University, Shanghai 200240, China*

[5]*Graduate School, China Academy of Engineering Physics, P.O. Box 2101, Beijing 100088, China*

(Received 17 April 2017; revised manuscript received 19 January 2018; published 11 May 2018)

We present the first experimental evidence supported by simulations of kinetic effects launched in the interpenetration layer between the laser-driven hohlraum plasma bubbles and the corona plasma of the compressed pellet at the Shenguang-III prototype laser facility. Solid plastic capsules were coated with carbon-deuterium layers; as the implosion neutron yield is quenched, DD fusion yield from the corona plasma provides a direct measure of the kinetic effects inside the hohlraum. An anomalous large energy spread of the DD neutron signal (∼282 keV) and anomalous scaling of the neutron yield with the thickness of the carbon-deuterium layers cannot be explained by the hydrodynamic mechanisms. Instead, these results can be attributed to kinetic shocks that arise in the hohlraum-wall–ablator interpenetration region, which result in efficient acceleration of the deuterons (∼28.8 J, 0.45% of the total input laser energy). These studies provide novel insight into the interactions and dynamics of a vacuum hohlraum and near-vacuum hohlraum.

DOI: 10.1103/PhysRevLett.120.195001

High-Z hohlraums are used to convert intense laser pulses or charged particle beams into soft x rays at a radiation temperature of hundreds of eV in indirect-drive inertial confinement fusion (ICF) [1,2]. Successful indirect-drive ignition requires highly symmetric implosion of a deuterium and tritium-filled capsule driven by these x rays. In order to minimize the motion of the laser deposition region and reduce the low-mode-number implosion asymmetries, low-Z gas filled hohlraums are used in the ignition campaign at the National Ignition Facility (NIF), the laser facility at the Lawrence Livermore National Laboratory (LLNL) [3]. However, the lack of control over the time dependence of the cross-beam energy transfer (CBET) within the gas filled hohlraums has led to a program to develop alternative near-vacuum hohlraums (NVHs) [4] or vacuum hohlraums [5] as a means of mitigating this issue. The reduction in the tamping effect of the gas introduces a new set of challenges into the design of NVHs. For example, the accurate simulation and comprehension of the observed low-mode drive asymmetry and loss of the inner-beam propagation [6].

In vacuum hohlraums (or NVHs), the high-Z plasma expands from the hohlraum wall and collides with the blowoff from the capsule (or the low-density fill-gas). Such a collision produces conditions in which kinetic effects may dominate since the ion-ion mean free paths are larger than the size of the interaction region. The formation and evolution of this inter-penetration region have been proposed as a cause for the symmetry discrepancy between NVH experiments and simulations [6], and lack of detailed interpenetration modeling in the code causes a density spike at the interface, which blocks inner-beam propagation [7]. Furthermore, strong electromagnetic field structures associated with the Au wall-gas diffusion layer have been observed in the hohlraum using proton radiography [8,9]. These kinetic effects, will have significant impact on the energy transport and other intrinsic plasma properties. In order to design and optimize our fusion target, it is necessary to know how kinetic effects impact on laser propagation and the potential for the late onset of low-mode drive asymmetry.

However, the kinetic processes stay quite unexplored in experiments and are not controlled. This is mainly due to two reasons [7]: (1) The time and length scales of kinetic physics quantities involved are on the order of picoseconds and microns, which are at the limit of the diagnostic resolution. (2) Even if kinetic physics significantly perturbs some aspect of plasma evolution, this does not necessarily imply unique kinetic effects are observable. For example, in vacuum hohlraums and NVHs, a kinetic electrostatic shock wave (ESW) [10] could be launched in the hohlraum-wall–ablator interpenetration region. The resulting observable

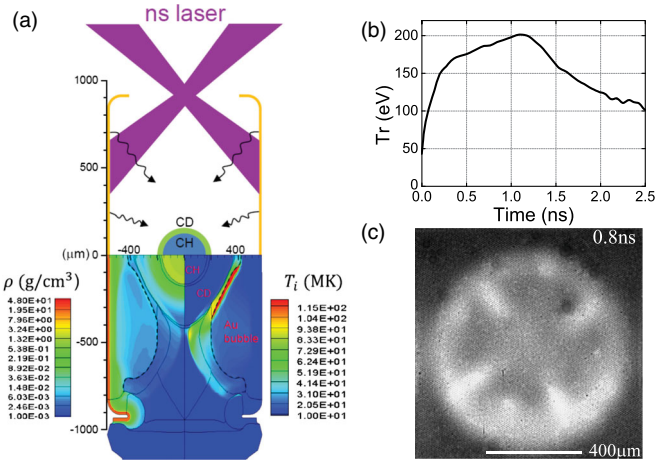

FIG. 1. (a) Schematic diagram of indirect-drive initial hohlraum target (up). Density profile (down, left) and ion temperature (down, right) at 0.8 ns from LARED-integration simulation. The solid CH capsule is used to suppress the implosion neutron, and the coated $CD_{1.4}$ layer (in this case, $CD_{1.4}$ thickness is 20 μm.) is used to convert the high energy ions into a measurable D-D neutron yield. (b) The temporal behaviors of radiation temperature measured by FXRD [12]. (c) The dynamics of the hohlraum captured by a gated x-ray detector along the polar axis at time $t = 0.8$ ns.

quantity tends to be the accelerated low-Z ions. However, even these ions are accelerated to tens of keVs, they still cannot penetrate the compressed core nor the hohlraum wall to reach the diagnostic devices.

The experiments described in this Letter demonstrate, for the first time, signatures of ESW accelerated ions in the hohlraum-wall–ablator interpenetration region, unveiling new aspects of the formation of the ESW and a possible source of low-mode drive asymmetry of the compressed pellet. We present, in detail, an overall situation that has never been described by radiation hydrodynamic (RH) simulations or experiments to our knowledge. Here, we used a solid CH ball, 360 μm in diameter coated with a layer of $CD_{1.4}$. The solid CH ball was used to suppress the implosion neutron, and the $CD_{1.4}$ layer was used to produce a measurable D-D neutron yield in supposing that deuterons can be accelerated in the hohlraum-wall–ablator interpenetration region. The advantage of employing a $CD_{1.4}$ layer is that the generated neutrons can penetrate through hohlraum and chamber walls. To the best of our knowledge, this is the first time that the kinetic effect in the hohlraum-wall–ablator interpenetration region has been demonstrated experimentally.

The experiments were performed at the Shenguang III-prototype laser facility at the Research Center of Laser Fusion in China. The hohlraum had a 25 μm thick gold wall, 0.8 mm diameter entrance holes, 1.85 mm length, and 1.1 mm diameter. Eight laser beams (0.8 kJ, 351 nm, 1 ns) were injected into the hohlraum at an angle of 45° relative to the hohlraum axis. The RH simulations performed with LARED-integration code [11] give an overview of the plasma conditions inside the hohlraum, as shown in Fig. 1(a). However, the interpenetration of the Au-CD plasma and kinetic physics inside cannot be properly described by these RH simulations. Radiation temperature was measured by a flat response x-ray detector [see Fig. 1(b)]. The yield and spectrum of the DD-fusion neutrons (2.45 MeV) via nuclear reaction $D(d,n)^3$He were measured by plastic scintillation neutron detector and a large array neutron spectrometer (LANS) with an energy resolution of 13 keV. These reactions can originate from (i) implosion of the CD capsules, (ii) hydrodynamic instabilities, (iii) stagnation heating of two streaming plasma due to ion-ion Coulomb collisions [13], or (iv) beam-target interaction of the high energy deuterons accelerated by kinetic ESW. In order to distinguish these individual components, a set of controlled experiments with four different thicknesses of the $CD_{1.4}$ coating layer of the pellet, i.e., 0.3 μm, 1.0 μm, 5.0 μm, and 20 μm, were used in experiments.

Figure 2(a) shows the measured neutron yields as a function of initial coating $CD_{1.4}$ thickness. One-dimensional RH simulations (open circles) were performed using the code RDMG for comparison to the observed values (solid circles). The measured yields show anomalous trends relative to the RH simulated values. The measured neutron yield increases with the thickness of the initial coating $CD_{1.4}$ and finally saturates. This trend cannot be explained by the implosion dynamics since the implosion neutron yield has been quenched by the solid CH ball used in our target design. Furthermore, the neutron yield is not due to hydrodynamic instability since this shock-driven implosion is insensitive to hydrodynamic instability growth for the present solid pellet case [14,15]. Actually, the estimation depending on the RH simulation and Thomson scattering showed that the ion-ion mean free paths of the interpenetration region are larger than the gradient length of the colliding front, a pure hydrodynamic description is certainly not enough to describe the physics. In this situation, both collisional effect and kinetic effect may play roles. It is therefore desirable to distinguish between these two effects with a set of controlled experiments.

The significance of ion kinetic effect and collisional effect in the hohlraum wall blowoff or ablator interpenetration regions can be assessed through measurements of the yield and spectrum of the DD fusion neutron [16]. A maximum yield of 7×10^7 was observed for the 20 μm thick CD coating case [case A in Fig. 2 (a)]. Besides, two specially coated pellets were used in order to provide a preliminary verdict as to whether kinetic effects are important: in case B, a thin CD coating with a thickness of 1 μm is used; in case C, a thick CD layer (thickness of 19 μm) is covered with another 1 μm CH layer outside. The shot of case B showed an average yield of 1.85×10^7, indicating 73.6% of the DD neutron yield from the deeper

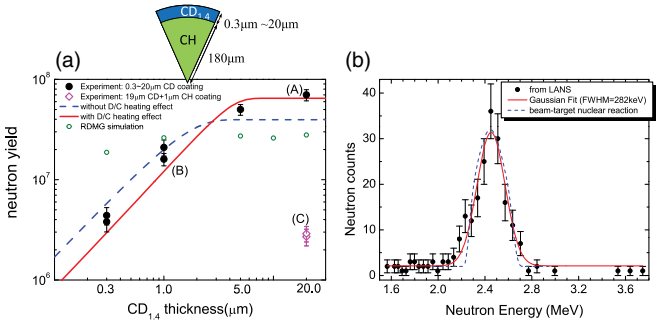

FIG. 2. (a) Neutron yields as a function of coating $CD_{1.4}$ thickness. The solid circles and magenta diamonds are experimental data. The red solid line is the results from Eq. (1) with ion heating effect, the blue dashed line represents those without ion heating effect. The open circles are from the RH simulations. (b) Measured neutron spectrum by the large array neutron spectrometer (solid circles). The solid line is the spectrum distribution fitted with a Gaussian profile, the dashed line is the spectrum distribution calculated based on the beam-target nuclear reaction.

region ($d > 1$ μm). In comparison, in case C, the yield dropped by a factor of ~25 to 2.8×10^6 (averaged) because of the 1 μm CH layer [magenta diamond in Fig. 2(a)]. The sum of the neutron yields in case B and case C is expected to be equal to that of case A if the ion-ion Coulomb collisions dominate, and a factor of 1.36 difference in yield between case C and case A is expected. Therefore, a factor of 25 yield reduction (to 2.8×10^6 in case C) in the data indicates that the dominant contribution to the yield is ion kinetic effects acting in the interpenetration region.

To highlight the kinetic effects, the measured neutron spectrum for the case with $CD_{1.4}$ thickness of 0.3 μm is plotted in Fig. 2(b). One can see that the spectrum has a quasi-Gaussian profile with an energy full width at half maximum (FWHM) of $\Delta E_{n,\mathrm{FWHM}} \sim 282$ keV (solid line). If the thermonuclear fusion dominates, we then assume that all species of the particles satisfy the Maxwell distribution with the same temperature, and the relationship between the neutron spectrum spread and the deuteron temperature T_a can be described as: $\Delta E_{n,\mathrm{FWHM}} = 82.5(kT_a)^{1/2}$ [17]. It gives $T_a \sim 12$ keV, which is much higher than those reported in ICF related experiments. Hence, a thermonuclear interpretation cannot explain this spread. We next analyze the possibility that a beam-target-type interaction could produce up to $\sim 10^7$ neutrons/sr, as a result of the formation of an ESW.

For a physical picture of the formation of the ESW, the expanding plasma bubbles generated on the hohlraum wall near the laser spots are governed by plasma hydrodynamics because the plasma thermal pressure is much higher than the magnetic pressure [8]. The plasma temperature and density of the expanding front have been revealed by the Thomson scattering and RH simulations. On the other hand, the ablated capsule material expands radially outward due to the x-ray ablation. When the high-temperature high density gold wall blow-off plasma collides with the low-temperature and low density CD plasma, a high pressure gradient is formed. Therefore, in vacuum hohlraum cases, the ESW is formed due to this pressure gradient at the hohlraum-wall–ablator interaction front [18,19]. Here, additional PIC simulations have been carried out to further illustrate our hypotheses.

We use the parallel electromagnetic PIC code ASCENT [20] to simulate the formation of the ESW. We send a nonrelativistic, supersonic Au plasma flow with velocity $v_x = 450$ km/s into a more rarefied CD plasma. The simulation box is divided along the x axis into two parts. The interval $-L_x/4 < x < 0$ contains the Au plasma with density $n_{e1} = 1.2 \times 10^{21}$ cm^{-3} and $Z_1 = 50$, whereas the interval $0 < x < 3L_x/4$ contains a CD plasma with density $n_{e2} = 4 \times 10^{19}$ cm^{-3}. The Au plasma has an electron (ion) temperature of 3–5 keV (0.1 keV). The CD plasma has an electron (ion) temperature of 0.1 keV (0.1 keV). In the simulations, we can see the formation of the ESW near the Au-CD interface, as shown in Figs. 3(a) and 3(b). The physics of the rapid formation of this ESW is quite straightforward: the high-temperature electrons of the Au plasma diffuse quickly into the CD plasma at the interface while the heavier Au ions are not able to keep up with this motion. Therefore, a positive electrostatic potential is set close to the Au-CD interface because of the charge imbalance, see Fig. 3(c). A fraction of CD ions are reflected by this electrostatic field, but some can cross this field and move downstream. Therefore, the accumulation of incoming upstream ions in the downstream reinforced the electrostatic potential. Finally, this nonlinear process leads to the formation of the ESW on the ion time scale [18,19]. The ESW propagates with a stable velocity of the order of the ion-acoustic speed of the heated CD plasma. As a result, in the shock rest frame, the CD ions are accelerated to an energy of the order of the electrostatic potential difference (~10 keV) between the downstream and the far upstream region by this ESW. In the Lab frame, the energetic deuterium and carbon ions have a high energy centered at ~25 keV and ~110 keV, respectively [see Fig. 3(d)]. Furthermore, since the plasma conditions in the hohlraum are difficult to precisely determine, additional collisional and collisionless PIC simulations with a wide range of initial plasma parameters have been carried out to further illustrate the physics. Under these plasma conditions, deuterium ions can be accelerated to energies of 16–29 keV.

Furthermore, the increasing and saturation trend of the measured neutron yield with the thickness of the CD layers [see Fig. 2(a)] can be interpreted as being due to the kinetic ESW which accelerates the high energy deuterons and causes a beam-target-type neutron reaction. This interpretation is supported by a close examination of the neutron yields caused by the high-energy deuterons inside the

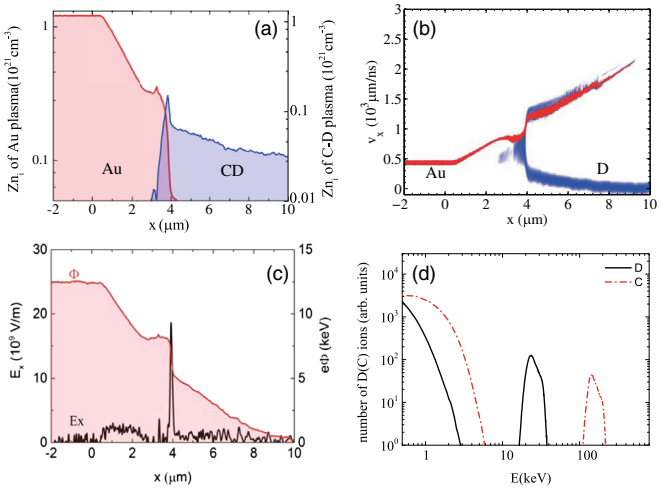

FIG. 3. (a) The density profile of Au and CD plasma from PIC simulations, (b) phase space plots $v_x \sim x$ of the Au-D ions, (c) electric field E_x and electrostatic potential Φ_x profile, and (d) energy spectrums of the CD ions within the precursor region. The PIC simulations were conducted with the ASCENT code and all the physical quantities are diagnosed at $t = 4.4$ ps. Physical quantities in (a),(b),(c) are averaged over the y direction, since the plasma expansion dynamics shows a one-dimensional feature predominantly.

$CD_{1.4}$ corona plasma. Detailed corona plasma conditions of a compressed solid ball is simulated by the 1D-RH simulation code RDMG [21]. As shown in Fig. 4(a), the $CD_{1.4}$ layers with different thickness are used to provide the source of the accelerated deuterons and also act as the converter to catch these accelerated deuterons for the beam-target nuclear reaction. The profiles of plasma density (ρ_{CD}) and temperatures (T_i) are given at $t = 866$ ps, when the CD corona plasma just contacts with the gold wall blow-off plasma. The density profile of the corona plasma has a typical exponential gradient. The ablated front edge of the $CD_{1.4}$ layer reaches $r \sim 470$ μm, and the $CH/CD_{1.4}$ interfaces move to the dashed-line marked positions [see Fig. 4(a)] for four different $CD_{1.4}$ thicknesses, respectively. After the gold wall blow-off plasma expands into this ablator blowoff, a large amount of deuterons are reflected and accelerated by the ESW (from PIC simulations), and finally return back and deposit into the compressed pellet. Thus, the neutrons are produced by the beam-target-type neutron reaction. We assume the deuterons undergo no angle scatter as they slow down and the nuclear reaction cross section is small relative to the atomic slowing down cross sections (neglecting the ion removal from the beam); the beam-target neutron yield can be approximately expressed as [22]

$$Y_n = N_{hD} \int_0^{\infty} f(E_{hD}) \left(\int_{E_{hD}}^{E'_{hD}} \frac{n_D(x(E_D))\sigma(E_D)}{dE/dx(E_D,T)} dE_D \right) dE_{hD}, \quad (1)$$

where $f(E_{hD})$ and N_{hD} are the normalized spectrum distribution and number of the accelerated deuterons. Here, $f(E_{hD})$ is obtained from the PIC simulations while N_{hD} cannot be given directly because of the 3D effect [see Fig. 1(c)] due to the limited laser beams of SG-III prototype. Here, N_{hD} was carefully adjusted to match all four experimental yields [shown in Fig. 2(a)] simultaneously with a fixed energy spectrum. $N_{hD} \sim 0.72 \times 10^{16}$ and a beam-target neutron spectrum [dashed line in Fig. 2(b)] are then obtained. This means about 28.8 J (~0.45%) high energy deuterons can be accelerated for the present case with a total laser energy of 6.4 kJ. $dE/dx(E_D, T)$ is the stopping power and it accounts for energy loss due to ionization, elastic scattering, electromagnetic fields, and the resistivity of the free electrons. $n_D = 1.4\rho_{CD_{1.4}} N_A/14.8$ is the number density of deuterons inside the corona plasma and σ is the cross section of the DD beam-target reaction. $E'_{hD} = E_{hD} - \int_{r_0}^{r_0-\delta} ([dE/dx])dx$ is the residual energy of high energy deuterons after passing through the ablator CD blowoff from the ablated front edge ($r_0 = 470$ μm). Here, E_{hD} is the initial energy of the high energy deuterons and δ is the thickness of the penetration depth inside the ablator CD blowoff. Taking into consideration the hydrodynamic evolution, the beam-target neutron yield (Y_n) as a function of the initial thickness of the $CD_{1.4}$ layer can be evaluated from Eq. (1), which is shown in Fig. 2(a) (the blue dashed line). Note that the neutron yield increases with the initial $CD_{1.4}$ thickness, and saturates after the thickness is larger than 3 μm due to the strong stopping power and the limited penetration depth for these accelerated deuterons. It is interesting to note that if we consider the ion heating effect, and account for the temperature enhancement of the ablator CD blowoff, the theoretical estimate matches the observed neutron yield more closely, as shown in Fig. 2(a). This is not surprising, as the stopping power becomes weaker with the heating effect, and more high energy deuterons can reach a deeper (higher density) region of the ablator CD blowoff. Furthermore, proton radiography has been used to confirm the possibility of the formation of the ESW at the SG-II upgrade laser facility. Here, the gold plane target was ablated by three long-pulse lasers at an angle of 40°. The CD target was ablated by radiation coming from the gold target. The proton beam was externally generated during the interaction of an ultraintense laser beam with a copper target. Figure 4(b) shows a very sharp shock structure, which is stabilized by ion reflection at the shock front. The ambient plasma parameters inferred from LARED-integration simulations indicate an ion-acoustic velocity of $c_s \approx 2 \times 10^5$ m/s implying that these velocities would correspond to a Mach number $M \sim 3.4$. We infer that this shocklike structure is collisionless and predominantly electrostatic.

In summary, the kinetic effect launched at the hohlraum-wall–ablator interpenetration layer was directly studied for the first time at the Shenguang-III prototype laser facility

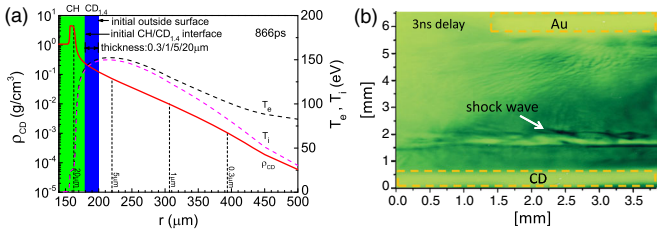

FIG. 4. (a) The density distribution of CD plasma (red solid line), electron temperature (black dashed line), and ion temperature (magenta dash-dotted line) distribution of CD plasma at 866 ps from RDMG-1D spherical model. The upright dashed lines represent the CH/CD plasma interfaces for 0.3 μm, 1.0 μm, 5.0 μm, and 20 μm initial $CD_{1.4}$ thicknesses. (b) Typical proton imaging data of the collision of the Au bubble with low-density CD plasma at the time 3 ns after the end of the long pulse laser. The proton beam was detected employing a stack of several layers of dosimetrically calibrated radiochromic films (RCFs).

using DD beam-target fusion reactions in implosions of solid plastic capsules with different thicknesses of the CD coated layer. Experimental data are consistent with PIC simulations showing that copious amounts of high energy deuterons reflected back by the ESW at the hohlraum-wall–ablator interpenetration layer enter into the ablator CD blowoff (as the deuterium substrate) and produce fusion neutrons via DD beam-target interactions. Hydrodynamic mechanisms have been ruled out as explanations for the observation, as they do not introduce a sufficient neutron yield in thick CD coated layer cases and do not show the clear trend that the experimental neutron yield obviously increases with the thickness of CD layer. It is found that accelerated deuteron and carbon ions take approximately ~0.45% and ~2% of the total input laser energy for the present experiments on the SG-III prototype, respectively. When these high energy ions were deposited inside the capsule, it resulted in significant low-mode asymmetry [6] of the implosion capsule since there are no high energy ions from the laser entrance holes. The evaluation of this impact on the capsule implosions will be considered in a future experiment with delicate target design.

This work was supported by the Science Challenge Project (No. TZ2016005) in China, the National Key Programme for S&T Research and Development (Grant No. 2016YFA0401100), the National Natural Science Foundation of China (Grants No. 11575030 and No. U1730449 (NSAF)), and China Academy of Engineering Physics Foundation (Grant No. 2014A0102003). H. B. Cai thanks Bo Yang and Bin Zhong for fruitful discussion. PIC simulations were performed on the Tianhe-2 supercomputer (China).

*cai_hongbo@iapcm.ac.cn
†yqgu@caep.cn

[1] J. Nuckolls, L. Wood, A. Thiessen, and G. Zimmerman, Nature (London) **239**, 139 (1972).
[2] J. Lindl, Phys. Plasmas **2**, 3933 (1995).
[3] E. I. Moses, and C. R. Wuest, Fusion Sci. Technol. **47**, 314 (2005).
[4] S. LePape *et al.*, Phys. Rev. Lett. **112**, 225002 (2014).
[5] F. Philippe *et al.*, Phys. Rev. Lett. **104**, 035004 (2010).
[6] L. F. Berzak Hopkins *et al.*, Phys. Rev. Lett. **114**, 175001 (2015); L. F. Berzak Hopkins *et al.*, Phys. Plasmas **22**, 056318 (2015).
[7] H. G. Rinderknecht, P. A. Amendt, S. C. Wilks, and G. Collins, Plasma Phys. Controlled Fusion **60**, 064001 (2018).
[8] C. K. Li *et al.*, Science **327**, 1231 (2010).
[9] C. K. Li *et al.*, Phys. Rev. Lett. **102**, 205001 (2009).
[10] L. Romagnani *et al.*, Phys. Rev. Lett. **101**, 025004 (2008).
[11] W. Pei, Commun. Comput. Phys. **2**, 255 (2007); P. Song *et al.*, High Power Laser Particle Beams **27**, 032007 (2015).
[12] Z. Li *et al.*, Rev. Sci. Instrum. **81**, 073504 (2010).
[13] O. Rancu *et al.*, Phys. Rev. Lett. **75**, 3854 (1995); T. Boehly *et al.*, Appl. Phys. B **50**, 165 (1990); O. Renner *et al.*, High Energy Density Phys. **9**, 568 (2013).
[14] H. G. Rinderknecht *et al.*, Phys. Rev. Lett. **112**, 135001 (2014).
[15] M. J. Rosenberg *et al.*, Phys. Rev. Lett. **112**, 185001 (2014).
[16] J. S. Ross *et al.*, Phys. Rev. Lett. **118**, 185003 (2017).
[17] H. Brysk, Plasma Phys. **15**, 611 (1973).
[18] G. Sarri, M. E. Dieckmann, I. Kourakis, and M. Borghesi, Phys. Rev. Lett. **107**, 025003 (2011).
[19] W. S. Zhang, H.-B. Cai, L.-Q. Shan, H.-S. Zhang, Y.-Q. Gu, and S.-P. Zhu, Nucl. Fusion **57**, 066012 (2017).
[20] H. B. Cai, K. Mima, W.-m. Zhou, T. Jozaki, H. Nagatomo, A. Sunahara, and R. J. Mason, Phys. Rev. Lett. **102**, 245001 (2009).
[21] X. T. He, J. W. Li, Z. F. Fan, L. F. Wang, J. Liu, K. Lan, J. F. Wu, and W. H. Ye, Phys. Plasmas **23**, 082706 (2016).
[22] L. J. Perkins, B. G Logan, M. D Rosen, M. D. Perry, T. D. de la Rubia, N. M. Ghoniem, T. Ditmire, P. T. Springer, and S. C. Wilks, Nucl. Fusion **40**, 1 (2000).